Atmospheric Environment 42 (2008) 8600–8615

Contents lists available at ScienceDirect

Atmospheric Environment

journal homepage: www.elsevier.com/locate/atmosenv

A regional scale chemical transport modeling of Asian aerosols with data assimilation of AOD observations using optimal interpolation technique

B. Adhikary [a,*], S. Kulkarni [a,1], A. Dallura [b,2], Y. Tang [b,3], T. Chai [b,4,5], L.R. Leung [c,6], Y. Qian [c,7], C.E. Chung [d,8], V. Ramanathan [d,9], G.R. Carmichael [a,10]

[a] Center for Global and Regional Environmental Research, and Department of Chemical and Biochemical Engineering, The University of Iowa, Iowa City, IA, USA
[b] Center for Global and Regional Environmental Research, The University of Iowa, Iowa City, IA, USA
[c] Pacific Northwest National Laboratory, P.O. Box 999, Richland, WA 99352, USA
[d] Scripps Institution of Oceanography, University of California at San Diego, La Jolla, CA, USA

ARTICLE INFO

Article history:
Received 21 April 2008
Received in revised form 14 August 2008
Accepted 19 August 2008

Keywords:
Aerosol transport modeling
Data assimilation
Receptor modeling

ABSTRACT

A regional chemical transport model assimilated with monthly mean satellite and ground based aerosol optical depth (AOD) observations was used to produce three dimensional distributions of aerosols throughout Asia for a period of four years. The model was evaluated with daily assimilation of AOD for the month of April 2005. Sulfur Transport dEposition Model (STEM), a regional chemical transport model, was used to simulate aerosol distributions at a resolution of 50×50 km with a time interval of 3 h. Monthly mean Moderate Resolution Imaging Spectroradiometer (MODIS) AOD along with AErosol RObotic NETwork (AERONET) AOD was used in an optimal interpolation assimilation scheme to yield regional distributions of aerosols. The MODIS AOD and aerosol fine mode fraction information (where available) were used in the assimilation technique. The daily assimilation of AOD results shows that the optimal interpolation algorithm is able to significantly improve model aerosol mass prediction skills at the two sites in Asia. Sensitivity studies were also conducted with different assimilation parameters on a daily assimilation scale and these results are discussed. The assimilation results of four-year aerosol fields were used to study the spatial and temporal distribution of aerosols in Asia. Two remote sites, Hanimaadhoo and Gosan were chosen as the case studies to study the outflow from the Indian subcontinent and East Asia. Seasonal and vertical structures of the

* Corresponding author. 407 IATL, Iowa City, IA 52242, USA. Tel.: +1 319 335 3335; fax: +1 319 335 3337.
E-mail addresses: badhikar@engineering.uiowa.edu (B. Adhikary), sarika-kulkarni@uiowa.edu (S. Kulkarni), alessio.dallura@gmail.com (A. Dallura), Youhua.Tang@noaa.gov (Y. Tang), Chai.Tianfeng@epamail.epa.gov (T. Chai), Ruby.Leung@pnl.gov (L.R. Leung), Yun.Qian@pnl.gov (Y. Qian), chul.chung@helsinki.fi (C.E. Chung), vram@ucsd.edu (V. Ramanathan), gcarmich@engineering.uiowa.edu (G.R. Carmichael).
[1] Present address: 431 IATL, Iowa City, IA 52242, USA. Tel.: +1 319 335 2063; fax: +1 319 335 3337.
[2] Present address: ARIANET Srl, Via Gilino n. 9, 20128 Milano, Italy. Tel.:+39 02 27007255; fax: +39 02 25708084.
[3] Present address: Meso-scale modeling, NOAA/NCEP/EMC, W/NP2, NOAA, WWB #207, 5200 Auth Road, Camp Springs, MD 20746, USA. Tel.: +1 301 763 8000x7250; fax: +1 301 763 8545.
[4] Present address: Atmospheric Sciences and Modeling Division, NOAA-EPA, U.S. Environmental Protection Agency, 109 T W Alexander Drive, Research Triangle Park, NC 27711, USA. Tel.: +1 919 541 3557; fax: +1 919 541 1379.
[5] On assignment from Science and Technology Corporation, 10 Basil Sawyer Drive Hampton, Virginia 23666.
[6] Tel.: +1 509 372 6182; fax: +1 509 375 6448.
[7] Tel.: +1 509 372 6404; fax: +1 509 375 6448.
[8] Present address: Division of Atmospheric Sciences and Geophysics, University of Helsinki, Finland. Tel.: +358 919151084.
[9] Tel.: +1 858 534 8815; fax: +1 858 534 7452.
[10] 428 IATL, Iowa City, IA 52242, USA. Tel.: +1 319 335 3333; fax: +1 319 335 3337.

1352-2310/$ – see front matter
doi:10.1016/j.atmosenv.2008.08.031

aerosols are presented at these two sites. Positive Matrix Factorization (PMF), a factor analytic method was also used to characterize the source profile and source contribution at these two locations. A three-factor solution was able to explain more than 80% of the variation in the individual species at Hanimaadhoo and 90% variation of aerosol loadings at Gosan. The four-year averaged PMF model results were able to capture the seasonality of anthropogenic and dust loadings at both these locations. In addition, the PMF model identified the differences in the composition of anthropogenic aerosols over Hanimaadhoo and Gosan reflecting the differences in regional emissions. The PMF derived factors could be used as additional constraints for future assimilation studies.

1. Introduction

The Intergovernmental Panel on Climate Change (IPCC) places a 'very high confidence' that human activities are contributing to global warming since 1750 (IPCC, 2007). The report also points out that while there has been greater understanding about the role that aerosol plays in climate change, they are still 'the dominant uncertainty in radiative forcing'. Aerosols can impact climate through direct and indirect processes. Light scattering, by particles containing sulfate, organic carbon and nitrate, can reduce visibility by 60–95% and absorption by soot can reduce visibility by 5–40% (Ramanathan and Carmichael, 2008; Jacobson, 2005). Several studies have shown significant adverse impact of aerosol particles on the earth's hydrological cycle (Ramanathan et al., 2001a), agricultural production (Chameides et al., 1999), and human health (Pope et al., 2002).

To evaluate the effects of aerosols on climate it is necessary to estimate their spatial and temporal distributions. Currently there are large uncertainties in the spatial and temporal distributions of aerosols. An important metric in the characterization of aerosol distribution is aerosol optical depth (AOD). AOD is defined as a column integrated extinction coefficient over a unit cross section. The aerosol extinction coefficient is a function of wavelength λ, and m, the particle refractive index. Recent satellite-based remote sensing of AOD has greatly improved our understanding of aerosols properties. A number of satellite-based instruments such as MODIS, MISR, TOMS and OMI provide aerosol observations; further details of satellite-based remote sensing are found elsewhere (IGAC, 2007). Because of its spatial and temporal coverage, satellite-based aerosol optical depth is the most practical measurement of aerosol amount for global assessments (Anderson et al., 2005). However, despite satellite-derived aerosol observations, there is a strong need for chemical transport model calculation of aerosol concentration because these satellite products do not reveal chemical composition or the emission sources needed for any effective mitigation strategy. Chemical transport models provide a means to link emissions with aerosol distributions, but are also uncertain due to uncertainties in emission sources, meteorology, and aerosol/chemistry processes (Kinne et al., 2006).

Data assimilation, an approach first used in generating initial condition for the numerical weather prediction, offers a means to reduce the uncertainties in the estimates of aerosol distributions. Several mathematical techniques of atmospheric data assimilation have been developed and their scientific basis is presented elsewhere (for e.g. Kalnay, 2003). Studies using data assimilation of observed atmospheric trace gases such as CO and ozone with mathematical models have been successful in obtaining better analysis (Jeuken et al., 1999; Khattatov et al., 2000; Lamarque et al., 2002; Chai et al., 2007).

Aerosol data assimilation using AVHRR satellite data into three dimensional chemical transport model was first introduced by Collins et al. (2001) for studying the INDOEX aerosols using the MATCH model. They used an optimal interpolation technique initially developed for meteorological applications (Lorenc, 1986) and trace gas species (Khattatov et al., 2000). Since then, several other researchers have assimilated satellite-derived aerosol observations to chemical transport models. Wang et al. (2004) used GEOS 8 derived aerosol observations to assimilate dust and sea salt aerosols in the RAMS model using a Newtonian nudging scheme. A 3D-Var method was used by Niu et al. (2007) to assimilate dust loading retrieved from Chinese geostationary satellite FY-2C (Niu et al., 2007). Both these models showed that the assimilation greatly improved analysis when comparing with independent observations. Yu et al. (2003) used the optimal interpolation technique described by Collins et al. (2001) to assimilate MODIS AOD with their global transport GOCART model (Yu et al., 2003). They used monthly MODIS AOD to assimilate GOCART monthly AOD calculations. Their results showed that the assimilated data were better correlated with surface AERONET AOD data when compared to either MODIS data alone or with just the GOCART modeled AOD.

In this paper we have used data assimilation to produce aerosol distributions with reduced uncertainties for the study region of Asia. These distributions are subsequently used in estimates of aerosol radiative forcing (Chung et al., submitted for publication). A four-year period is simulated so that individual aerosol loading as well as their interannual variability can be analyzed. Further, the paper explores the technique of combining forward (satellite and chemical transport) and backward (receptor) modeling approaches to study the distribution of aerosols at two sites with different emission sources. This technique may be further refined and used in future assimilation in an iterative process to get better constrained aerosol distributions.

The paper is organized as follows: we first describe the assimilation technique, and then describe our regional 3D chemical transport model along with assimilation algorithm used. We then describe the availability and usage of satellite and other observation data in our study. Next, we present

the methodology of our receptor modeling technique. In the results section, we first present the assimilated model AOD evaluation and sensitivity to different model parameters. Then we present the regional distribution of the aerosols based on a four-year simulation. Finally, we discuss the results of combined forward and backward models in describing aerosol characteristics at two locations.

2. Methodology

2.1. Aerosol data assimilation

We implemented an optimal interpolation technique similar to the methodology described by Collins et al. (2001) for INDOEX aerosols using their MATCH model. The mathematical relationship between the posterior aerosol distribution (analysis) with the model predicted aerosol (background) and satellite-based observation (observation) is:

$$\tau'_m = \tau_m + K(\tau_o - H\tau_m). \quad (1)$$

τ'_m is the posterior aerosol optical depth while τ_o, and τ_m, are the observed and modeled AOD, respectively. K is the Kalman gain matrix and H is a linear interpolator from model space to observation space. Since we transform the observation AOD into the same model grid as the STEM model grid, the H matrix is simply the identity matrix. K matrix is calculated based on the background and observation error covariance matrices and is defined by Eq. (2).

$$K = BH^T\left(HBH^T + O\right)^{-1} \quad (2)$$

B and O are the error covariance matrices of background and the observation fields, respectively. Detailed discussion and assumption used to derive the B and O matrices are discussed elsewhere (Khattatov et al., 2000; Collins et al., 2001). In Eqs. (3) and (4) we simply restate the mathematical relationship defining B and O matrices such that outcome of the sensitivity studies discussed in Section 3.1 may be better understood.

$$O = (f_o\tau_o + \varepsilon_o)^2 I \quad (3)$$

ε_o is the minimum Root Mean Square (RMS) error of the observation and f_o is the fractional error in observation AOD.

$$B_{ij} = (f_m\tau_m + \varepsilon_m)^2 \exp\left[-\frac{d_x^2 + d_y^2}{2l_{xy}^2}\right] \quad (4)$$

ε_m is the minimum RMS uncertainty in the modeled AOD. f_m is the fractional error in the model AOD. Variables d_x and d_y are the horizontal distances between two model grid points i and j, and l_{xy} is the horizontal correlation length scale for errors in the model fields.

2.2. Chemical transport model description

The Sulfur Transport dEposition Model (STEM-2K1, hereafter referred to as STEM) was used to generate three dimensional aerosol distributions from 2001 to 2004 and for April 2005. The April 2005 assimilation is used for model validation and to conduct sensitivity experiments with tunable assimilation parameters. The STEM model has been used previously to study aerosols and trace gases during the same time period over South and South East Asia (Carmichael et al., 2003; Tang et al., 2004; Guttikunda et al., 2005; Adhikary et al., 2007). This is the first application of the STEM model to simulate high resolution (both spatial and temporal) aerosol concentration over multiple years so that the averaged annual aerosol distribution with inter-annual variability can be analyzed. The STEM 3D model has a horizontal resolution of 50×50 km. The model altitude ranges from the surface to a height of about 14 km with 23 layers in between. The STEM model utilizes USGS land use 25 categories to model land use dependant variables. The model is simulated with output generated at every 3 h. Geographically the model domain ranges from 20S to 50N latitude and from 40E to 140E longitude.

The meteorological model used for this study was the PNNL-MM5 model. Further details of the PNNL-MM5 meteorological model parameters and the STEM model are discussed by Chung et al. (submitted for publication) and Adhikary et al. (2007). Anthropogenic emissions inventory used in this study was primarily from the emissions inventory developed for TRACE-P intensive field campaign (Streets et al., 2003). The resolution of this emission inventory was 0.5×0.5 degrees for area sources and actual physical location for the large point sources. Since this modeling domain is bigger than TRACE-P domain, emissions data from EDGAR database and global black carbon (BC) and organic carbon (OC) emissions estimate from Tami Bond et al. were used to fill the extended geographical areas (Olivier and Berdowski, 2001; Bond et al., 2004). Monthly varying BC and OC emissions from biomass burning were included in this study based on published emissions data (van der Werf et al., 2006). The resolution of the biomass burning emissions inventory is 1×1 degree, which was then interpolated to our model grid. Secondary sulfate aerosols were calculated using a parameterized equation for its formation from SO_2. This methodology has been able to capture the seasonality and magnitude reasonably well in Asia (Uno et al., 2003; Adhikary et al., 2007). Carbonaceous aerosols were allowed to age with a fixed ageing time converting them from hydrophobic to hydrophilic aerosols. Hydrophilic aerosols were subject to wet scavenging by precipitation while hydrophobic were only dry deposited. The emissions of sea salt were calculated based on the parameterization of Gong (2003). Dust emissions were calculated online based on the methodology discussed by Tang et al. (2004). The emissions of carbonaceous and sulfate aerosols were assumed to be in the sub-micron range (diameter < 1 μm) and were not further resolved into any size bins. Sea salt emissions were calculated for four different size bins. However, during transport they were modeled as fine mode (<2.5 μm) and coarse mode (2.5 μm $<$ diameter < 10 μm). Dust transport was modeled using two size bins: submicron and super micron (1 μm $<$ diameter < 10 μm).

2.3. Assimilation algorithm

The STEM model was used to calculate three dimensional aerosol concentrations. The aerosols modeled and subsequently impacted by assimilation are sulfate, BC, OC, sea salt and mineral dust. The model does not calculate secondary organic aerosol (SOA) or nitrate aerosols. The aerosol mass distributions obtained from STEM were then used to calculate AOD using chemical species-specific extinction information. The extinction coefficient parameters used in the STEM model are reported in the paper by Penner et al. (2001). Two dimensional distribution of AOD was then used as the background field for the optimal interpolation algorithm discussed previously. The observation-based AOD distribution was then compared with the background AOD.

The data assimilation technique was conducted for both daily and monthly time steps. The four-year simulation utilized monthly average values. The technique of using monthly assimilated satellite data has been previously employed by Yu et al. (2003) to study the annual aerosol distribution and its impact on radiative forcing. By simulating and assimilating observations for more than a year, we were able to study the multiyear averaged spatial distribution and analyze the inter-annual variability. The assimilation algorithm is as follows: first, the STEM model calculated three dimensional aerosol concentrations every 3 h for all four years. This data was then averaged to produce a monthly three dimensional aerosol concentrations and monthly AOD. The STEM model generated AOD was then used for assimilation with observed AOD derived from MODIS and AERONET AODs. The B (Eq. (3)) and O (Eq. (4)) matrices are calculated using the parameters provided by Collins et al. (2001) study. We then calculate the K matrix (Eq. (2)) at each assimilation step. We propagate the updated mixing ratios forward in time for the daily assimilation case; however, for the multiyear monthly assimilation we do not.

Our methodology differs from Collins et al. in that our assimilation algorithm impacts sea salt distribution while their work chose to keep the modeled sea salt distribution fixed. Another difference in our assimilation technique from Collins et al. (2001) and Yu et al. (2003) is that we utilize both the coarse mode and fine mode AOD available from MODIS data. Coarse mode AOD was calculated from total AOD (which was available) minus the fine mode fraction. In our assimilation methodology, when there was no fine mode fraction available at the model grid point, the assimilation was done using the total AOD. So our observation vectors are fine mode AOD and coarse mode AOD/total AOD. Our background vectors are modeled fine mode AOD (sulfate-AOD + BC-AOD + OC-AOD) and modeled coarse mode AOD (dust-AOD + sea salt-AOD). At each time step, our assimilation impacts the concentration of anthropogenic aerosols namely sulfate, black carbon and organic carbon linearly based on the ratio of assimilated fine mode AOD to background AOD. Similarly, at each time step the concentration of dust and sea salt (regardless of the size distribution) was adjusted linearly based on the ratio of assimilated coarse mode/total AOD to background coarse AOD.

2.4. Observation data description

Satellites provide a variety of aerosol related parameters that can be used to constrain aerosol distributions. In this paper the observation data is the Moderate Resolution Imaging Spectroradiometer (MODIS) aerosol optical depth. For the daily data assimilation case, we obtained from the LAADS (Level 1 and Atmosphere Archive and Distribution System) website, Level 3 Terra MODIS Collection 4 AOD data at 550 nm wavelength products over the ocean and continent at the spatial resolution of 1×1 degree. The data was then interpolated to our model resolution. The time series comparison of assimilated MODIS AOD was done against AErosol RObotic NETwork (AERONET) sun photometer AOD obtained from the AERONET website. We do not integrate AERONET sun photometer AOD into the MODIS AOD observations for the daily assimilation run during April 2005. For the four-year run, the MODIS and AERONET observations were integrated into the same observation field, this integration methodology is presented in detail in Chung et al. (2005). Total AOD and fine mode fraction information from MODIS were used for both the daily assimilation and the four-year monthly assimilation. Mass measurements of total particulate matter at Kathmandu, Nepal, and Hanimaadhoo, Maldives, were obtained from the Atmospheric Brown Cloud Project described in detail elsewhere (Ramanathan et al., 2007; Stone et al., 2007).

2.5. Receptor modeling algorithm

PMF (Positive Matrix Factorization), a form of factor analytic method, has been widely used in the atmospheric field for source apportionment studies involving ambient concentration measurements with unknown source profiles (Lee et al., 1999; Paterson et al., 1999; Polissar et al., 1999; Chueinta et al., 2000; Kim et al., 2005). The aim of PMF is to obtain two matrices G and F, which explain the variation in the data set X, a matrix, consisting of n number of observations and m chemical species. Mathematically,

$$X = GF + E \tag{5}$$

Where, G is an n by p matrix of source contributions describing the temporal variation of the sources, F is a p by m matrix of source profiles and E represents the unexplained data variance by the model. PMF solves Eq. (5) using an explicitly weighted least square approach and minimizes the objective function $Q(X, \sigma, G, F)$ defined as:

$$Q = \frac{\|X - GF\|_F^2}{\sigma} = \sum_{i=1}^{n} \sum_{j=1}^{m} \left(\frac{x_{ij} - \sum_{h=1}^{p} g_{ih} f_{hj}}{\sigma_{ij}} \right)^2 \tag{6}$$

$\|X - GF\|_F^2$ denotes the Frobenius norm of E and σ which is the known matrix of error estimates.

These error estimates (σ) of individual data points are used to determine the weights of the least square fit on the data matrix. The G (source contributions) and i (source

profiles) are determined so that the Frobenius norm of E divided by σ at each time step is minimized.

The PMF output also produces a matrix called Explained Variation (EV), which summarizes the relative importance of each factor in explaining the variability of different species in the PMF input; i.e., a large EV value of a species in a factor indicates that this particular factor explains a major portion of that species variability. EV is represented as a matrix of dimensions $p+1$ by m (similar to F matrix dimension but with one extra row $(p+1)$), which is a measure of how much variation in a species remains unexplained by the PMF solution. The EV values range from 0 (no variance explained) to 1 (100% variance explanation). PMF modeling guidelines suggested that if any value on the $(p+1)^{\text{th}}$ row exceeds 0.25, it indicates that species corresponding to that row is practically not explained. The details of the EV calculation are found elsewhere (Juntto and Paatero, 1994; Lee et al., 1999; Paatero, 2000). In this study, the input variables used in the PMF analysis are assimilated monthly mean AOD values of SO_4, BC, OC, coarse mode sea salt (SSC), fine mode sea salt (SSF), coarse mode dust (dust C) and fine mode dust (dust F) obtained from the four-year model simulation. The data error estimates were assumed to be 25% of the model predicted AOD. The sensitivity of the PMF solution to this error assumption was not evaluated and may be assessed in future studies. The PMF solution was obtained by trial and error until physically realistic sources were obtained, while simultaneously minimizing Q value as the principal criterion. The total AOD was regressed against the G matrix to obtain the source profiles (AOD ratio) and contributions (AOD) in terms of AOD units. The PMF results obtained for two different sites are described in Section 3.4.

3. Results and discussion

3.1. Case study: analysis for April 2005

To illustrate the assimilation procedure and to evaluate its impact on aerosol distributions we first discuss the assimilation results conducted for the month of April 2005. The spring months (March, April, May) are a good time to study aerosol characteristics in Asia because of high aerosol loading. Several experimental field campaigns such as ACE-Asia, TRACE-P, INDOEX, ABC-EAREX and PACDEX have been launched during this time period to study the continental Asian aerosols and their outflow (Ramanathan et al., 2001a, b; Carmichael et al., 2003; Huebert et al., 2003; Stith et al., submitted for publication). The episodic emissions of mineral dusts and other aerosols from biomass burning in the spring season provides another motivation to study assimilation during this time as the emissions for these sources are highly uncertain. April 2005 was used to test our daily data assimilation technique. Fig. 1 shows the STEM modeling domain used in this study and also shown are six AERONET stations (spanning across the domain), where AOD data was available for more than twenty days in April 2005. Fig. 1 also shows the location of the two ABC sites where aerosol mass measurements were available for April 2005.

Fig. 2 shows the time series of assimilated AOD at the AERONET sites along with the STEM modeled background

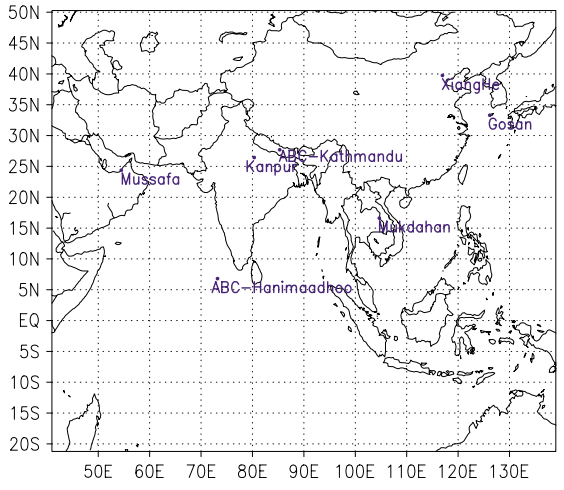

Fig. 1. Modeling domain and observation stations.

AOD. The figure also shows the time series of the MODIS data used in the assimilation and the AERONET AOD. These AERONET AOD data are independent observations, since we do not integrate them within the MODIS data, and thus can be used to evaluate the predicted values. For this run (Run 1) the values of the tunable parameters in Eqs. (3) and (4) are as follows: $\varepsilon_o = 0.04$, $f_o = 0.5$, $\varepsilon_m = 0.0$, $f_m = 0.5$ and $l_{xy} = 50$ km. Analyzing Fig. 2 it is seen that the daily assimilation of AOD using optimal interpolation improves the model predictions. The background model predictions were generally over predicting the observations, which the assimilation corrects for and brings the AOD values after assimilation closer to the AERONET observations. The temporal coverage of the MODIS observations at a given point range from ~30 to 70% for the month shown. Yet the information content in the surrounding geographical areas is significant as the neighboring grid cells information gets propagated to the current grid cell at a later time through the assimilation. This is illustrated for the results at Hanimaadhoo, where the assimilation results in a significant reduction in predicted AOD at the beginning of the month, where the site specific MODIS AOD had limited temporal coverage. The assimilated AOD matches closely with the independent AERONET values as shown in the figure. A significant limitation of the assimilation technique is shown under conditions where the MODIS AOD values have large errors (as evaluated against the AERONET AOD) as illustrated at Mukdahan. The assimilation forces the predictions to better match the MODIS observations, which differ significantly from the AERONET observations. This problem can be reduced by correcting the MODIS values using AERONET data before assimilation (as is done for the long-term assimilations discussed in the next section).

We also evaluated the impact of the assimilation of AOD on the prediction of particulate matter (PM) mass concentrations at the surface. PM mass data is available from the Atmospheric Brown Cloud (ABC-project) at two sites in Asia. The two ABC observatories are located at Kathmandu, Nepal, and Hanimaadhoo, Maldives. The impact of the assimilation of MODIS AOD on the prediction of $PM_{2.5}$ mass (sum of modeled sulfate, BC, OC, fine mode

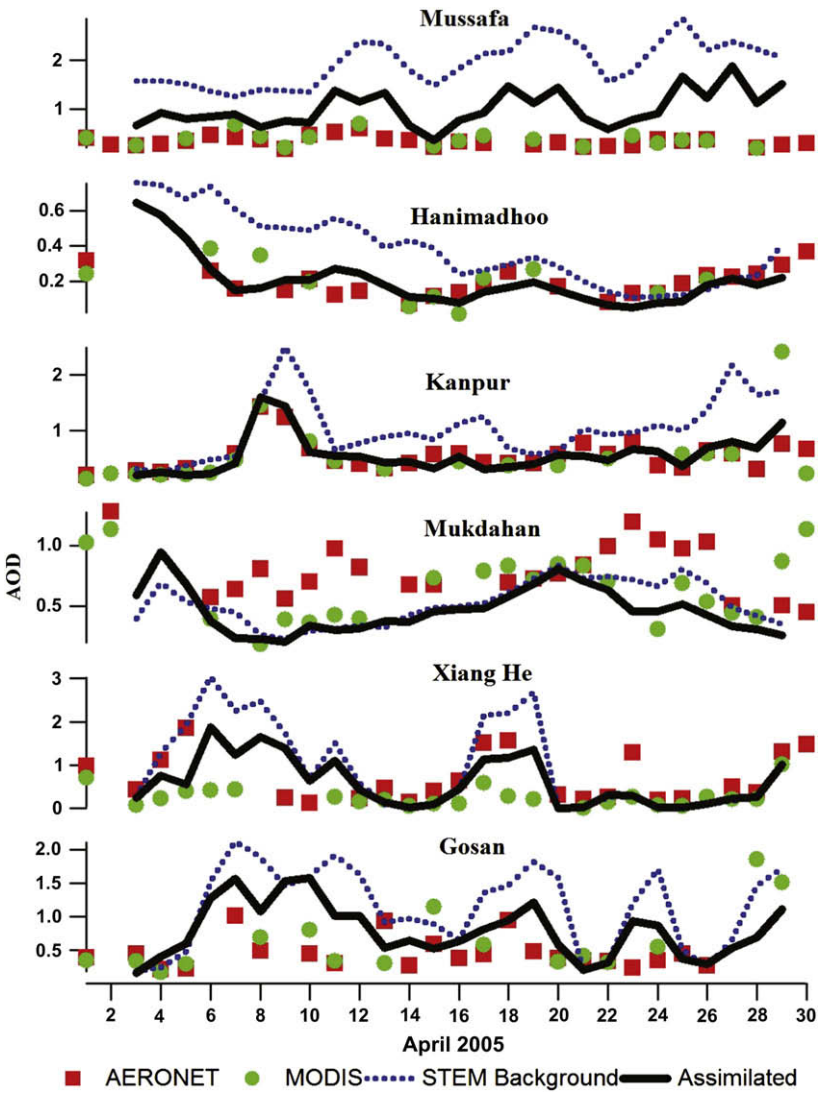

Fig. 2. Comparison of AERONET, MODIS, STEM background and assimilated AOD.

dust and fine mode sea salt) at Hanimaadhoo and Kathmandu is shown in Fig. 3. The figure shows that the assimilation results in $PM_{2.5}$ mass predictions that are much closer to the observed values. At Hanimaadhoo, the STEM-assimilated model was able to match the observations well after the first few days. During the first few days there were no MODIS data over Hanimaadhoo and the surrounding areas were laden with high dust in the background field. The STEM-assimilated Kathmandu $PM_{2.5}$ concentration also shows an overall improvement compared to the background model results.

The information obtained in the fine mode AOD fraction is important as it enables separate adjustments of the fine and coarse modes. The ratio of predicted fine mode AOD to predicted coarse mode AOD is shown in Fig. 4 for Hanimaadhoo and Kanpur, along with the observed AERONET angstrom exponent, a qualitative indicator of aerosol size. The impact of including the fine mode component in the assimilation is shown at Hanimaadhoo by comparing the results after assimilation to the predicted ratios for the background simulation. The temporal variations in the assimilated fraction of fine mode AOD ratios are shown to closely match the variation of the relative amounts of fine and coarse aerosol as reflected by the angstrom exponent.

A series of sensitivity simulations were performed to evaluate the effectiveness of the assimilation method and the results are summarized in Table 1. Comparing the root mean square error (RMSE) of the background and the assimilated model runs it is seen that the assimilation significantly reduces the errors (i.e., the RMSE was reduced by ~50%). A large uncertainty in predicted AOD is associated with the estimation of the size-resolved dust emissions. In the base assimilation run, dust in both the fine and coarse mode was adjusted using coarse mode AOD, to account for the large uncertainties in absolute dust emissions and the fine mode fraction in the emissions. An additional assimilation was done where fine mode dust was adjusted along with BC, sulfate and OC, using the

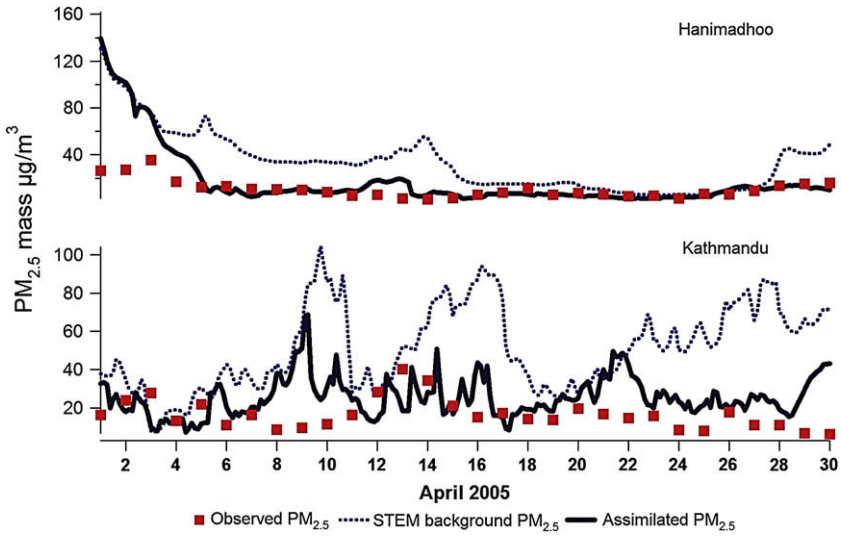

Fig. 3. Comparison of $PM_{2.5}$ mass at ABC stations.

MODIS fine mode fraction (Run2) and the RMSE in the assimilated results at individual sites ranged from 0.063 to 0.710. The impact of the assimilation of MODIS fine mode AOD on the prediction of total AOD was also evaluated by performing an assimilation using only the total AOD. The impact on RMSE at the various sites varied from 0.064 to 0.722. But as discussed above the fine mode information has a big impact on predicted $PM_{2.5}$ mass.

Three different sensitivity tests (Run4–Run6) were run that focused on the sensitivity of the results to the assimilation parameters. The first sensitivity test assumed the fractional error in the model to be equal to 0.1 instead of the 0.5. The second test was run assuming the fractional error in the model to be equal to 1.0. The third sensitivity test increased the values of l_{xy}, the horizontal correlation length scale for errors in the model fields to 150 km, which is three model grid cells. The results show that the differences in the magnitude of RMSE values were not significantly different within the range of parameters explored. Generally the results of the RMSE for the different assimilation algorithm varied by ~10% at different AERONET stations.

As discussed above and in Adhikary et al. (2007) the online dust emissions model used in STEM tends to over predict dust emissions (especially in South Asia), resulting in a systematic high bias in dust. One method to deal with this is to apply a uniform bias correction to the predicted dust. (A preferred method is to develop a more accurate dust emissions model and that is the

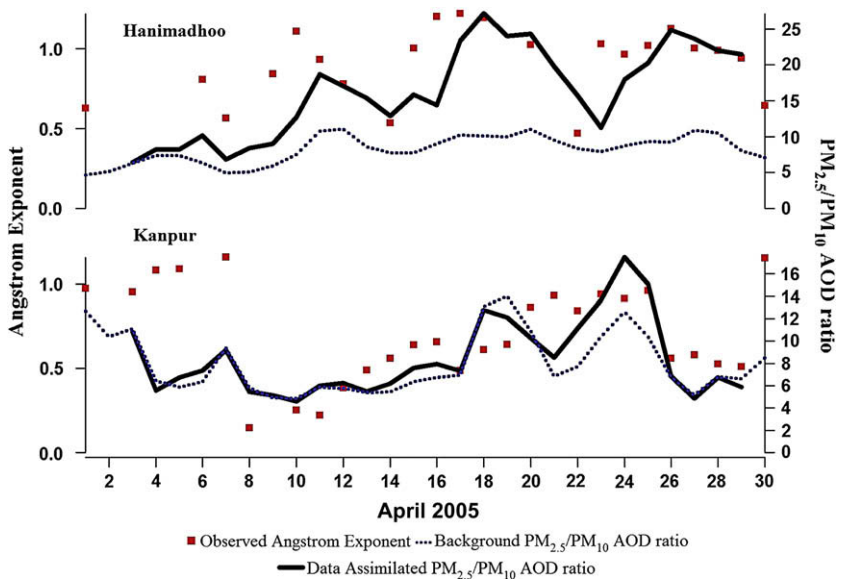

Fig. 4. Comparison of observed angstrom exponent with modeled aerosol size ratio.

Table 1
Change in model predicted daily AOD values at the AERONET sites from different data assimilation runs

	No assimilation	Run1	Run2	Run3	Run4	Run5	Run6
1 Mussafa	1.624	0.689	0.710	0.722	0.703	0.706	0.635
2 Kanpur	0.666	0.168	0.158	0.169	0.178	0.189	0.175
3 Hanimaadhoo	0.249	0.065	0.063	0.064	0.088	0.065	0.063
4 Mukadhan	0.317	0.223	0.187	0.263	0.115	0.256	0.344
5 XiangHe	0.496	0.502	0.518	0.499	0.499	0.496	0.543
6 Gosan	0.908	0.509	0.373	0.461	0.433	0.538	0.514
Average of all 6 stations	0.710	0.359	0.335	0.363	0.336	0.375	0.379

Run1: base data assimilation run; Run2: data assimilation with dust concentration scaled from fine mode fraction comparison; Run3: data assimilation without separation of fine mode/Coarse mode fraction from MODIS; Run4: sensitivity run changing the value of $f_m = 0.1$ and rest as base case; Run5: sensitivity run changing the value of $f_m = 1.0$ and rest as base case; Run6: sensitivity run changing the l_{xy} to 150 km and rest as base case.

long-term goal.) However, the assimilation of the MODIS AOD provides a means to bring in spatial and temporal variability. This is shown in Fig. 5, where predicted AOD at Kanpur is shown for the background simulation, and for simulations using a bias correction and assimilating MODIS AOD. Dust bias was corrected by constraining modeled dust concentration with a yearlong aerosol mass observations obtained from the ABC-project. Details about this bias correction are discussed in Adhikary et al. (2007) but it resulted in reducing the dust emission coefficient by 3.25 for South Asian application. Bias correction does a good job in improving the overall predictions, but must maintain the variability captured in the background model (which is quite good as indicated by the comparison of the observed and predicted temporal variability). However, the assimilation enables a closer temporal and spatial representation of aerosol distributions. This is shown for the period 6–10 April. The background model captures the main features of a dust event, but the impact of this event at Kanpur is ~2 days too late. The assimilation results adjust for dust upwind of Kanpur that were underestimated in the forward model, resulting in a good correspondence of the AOD temporal trends. Note that this happens even though the MODIS observations are limited at Kanpur during this period as shown in Fig. 2.

3.2. Regional AOD distributions

Fig. 6 shows the mean annual total and fine mode AOD averaged over the years 2001–2004. For these results the monthly assimilation algorithm with the base run (Run1) parameters was used. Also shown are the mean MODIS with AERONET corrections total- and fine mode AOD (i.e., the data used in the assimilation). The regions with the highest mean AOD from the MODIS data are located over the heavily polluted regions (including eastern China and Ganges valley of India), around the desert regions of western China and the Middle East, and the areas with large amounts of biomass burning (e.g., South East Asia). The assimilated AOD distributions follow closely these general patterns. The largest differences were seen in the desert regions where there is a lack of MODIS data to constrain the predicted values. The uncertainties of AOD results over these desert regions are very high because of lack of MODIS/AERONET observations. As discussed previously, dust emissions are highly uncertain and vary by a factor of 3–5 times from model to model (Bates et al., 2006). A previous study by Adhikary et al. (2007) found that the STEM model was over predicting the dust concentration by a factor of 3.25

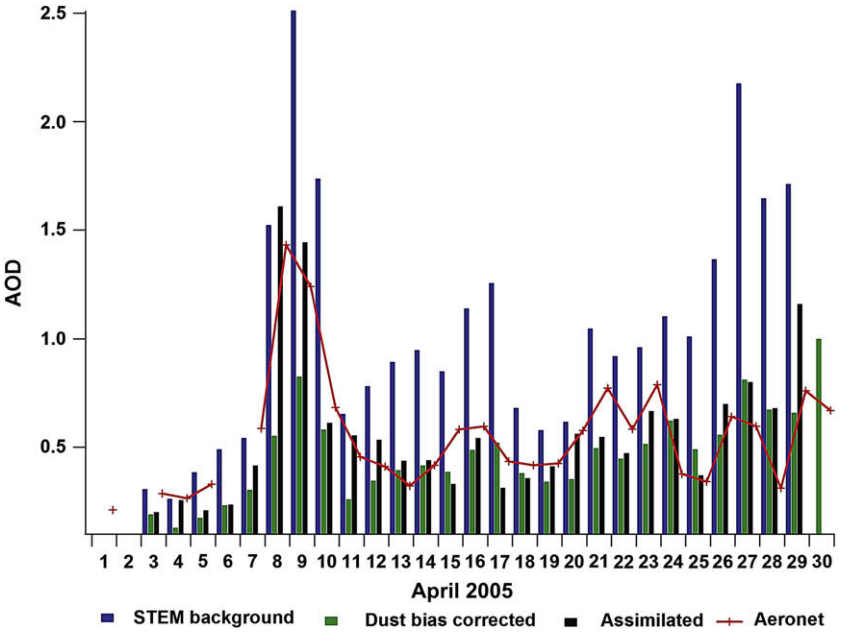

Fig. 5. Comparion of STEM background, bias corrected and assimilated AOD with observation.

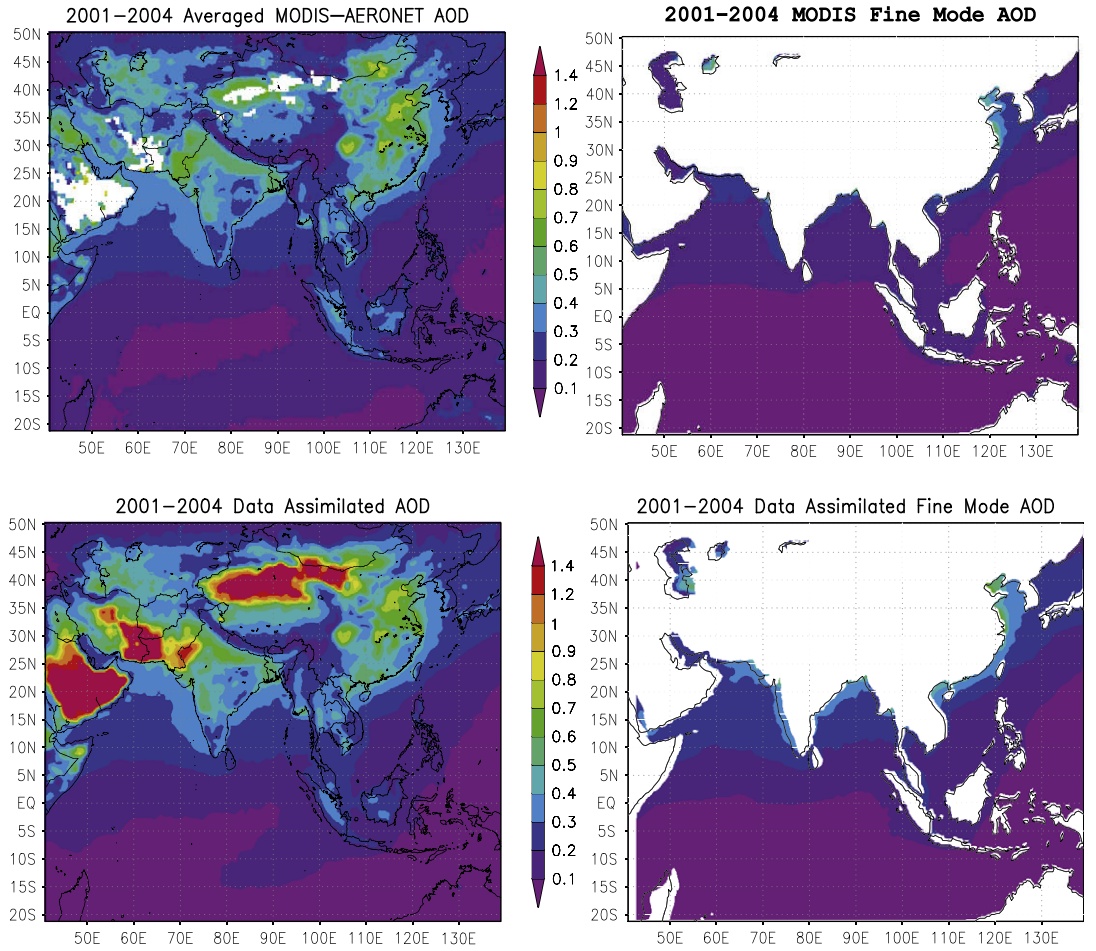

Fig. 6. Four-year averaged MODIS and assimilated AOD.

over the South Asian region. Future assimilation studies will need to use MODIS AOD retrieved using the 'Deep Blue Algorithm' as published studies have shown this retrieval is able to obtain AOD over desert surfaces (Hsu et al., 2006).

A comparison of the fine mode AOD is also shown in Fig. 6. Only the regions over the oceans are shown to compare the results more easily. Furthermore, the MODIS fine mode fraction data was available only over ocean regions for the four-year period simulated. The mean assimilated fine mode fraction matches closely the spatial distribution of the MODIS values, but with a tendency to be higher (e.g., the Arabian Sea region with assimilated fine mode AOD exceeding 0.2 in South Asia extends $\sim 5^{\circ}$ further south than the MODIS values).

The inter-annual variability in data assimilated fine mode AOD is shown in Fig. 7a, expressed in terms of coefficient of variation (CoV) (standard deviation of the annual means divided by the four-year mean). The regions with the highest variability were found where aerosol emissions are highly variable (i.e., over dust source regions and regions with active biomass burning). Both sources have strong inter-annual signals in their emissions. Significant inter-annual variability is also shown in the aerosol outflow regions (e.g., off the coast of Yellow Sea of China), which reflects inter-annual variability in upstream emissions and in removal rates due to variability in precipitation. Some high AOD regions have low variability. For example, the Ganges valley region over India shows a low CoV, indicating the strong aerosol layer is persistent over this region in all the years. This result is consistent with another study which showed a strong and persistent aerosol loading over this region in the winter months (Gautam et al., 2007), and which is shown clearly in the calculated CoV for the December, January and February (DJF) months (Fig. 7b). In Fig. 7a, the desert regions of China and Mongolia show high seasonal CoV mainly because of fine mode dust contribution to AOD. The availability of MODIS AOD over these regions varies with year and season. However, the CoV is low for desert regions of the Middle East mainly due to lack of MODIS data throughout the 2001–2004 periods. The high CoV over the South East Asia reflects seasonal emissions, dominated largely by biomass burning, and meteorology dependant removal processes.

Absorbing aerosols play an important role in climate change and their relative importance varies by region

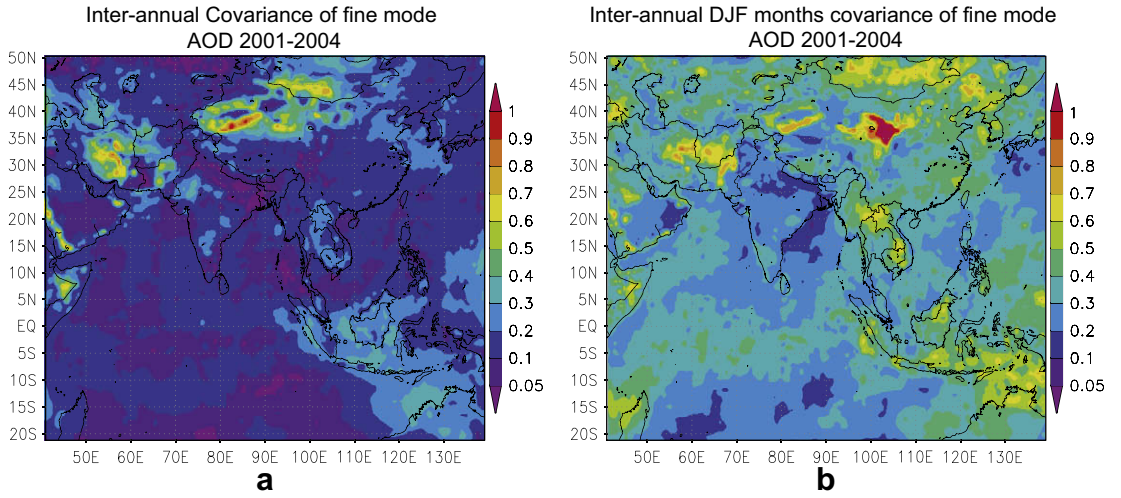

Fig. 7. Inter-annual and inter-annual DJF months covariance of fine mode AOD.

(Ramanathan et al., 2007). This is shown in Fig. 8a, where the geographical distribution of the four-year average BC to SO_4 AOD ratio is presented. The highest BC ratios occur over India and South East Asia. These patterns reflect the underlying emissions as shown in Fig. 8b. The high BC ratios over South Asia reflect the large contribution of biofuel use in the Indian subcontinent, while the high BC ratios over South East Asia are indicative of strong open biomass burning.

The spatial variability in the aerosol distributions is shown in Fig. 9, where four-year averaged vertical cross sections at a fixed latitude and longitude are presented. The two chosen cross sections slice through the middle of the polluted regions of mainland China and the Indian subcontinent. These cross sections are also chosen to supplement the discussion on radiative impact calculations presented in a companion paper by Chung et al. (submitted for publication). Fig. 9a shows the longitudinal gradient along 35N for mineral dust AOE. The highest dust AOE can be found at longitudes near the Taklimakan and Gobi deserts (80–100E) and the deserts of central Asia (50–60E). Elevated dust plumes are shown off mainland China at 126–133E transported from source regions and reaching altitudes up to ~8 km. Fig. 9b shows the BC AOE at 35N latitude (sulfate AOE shows similar structure (not shown)). BC-AOE has a different longitudinal gradient and vertical structure. Most of the BC-AOE is towards the Eastern China coast, South Korea and Japan, reflecting the geographical distribution of anthropogenic BC emissions. Fig. 9c shows the dust-AOE along 76E longitude. The results show that the dust AOE increases towards the north, reflecting emissions from Western India and central Asia. Fig. 9d shows the vertical structure of the sulfate AOE along 76E. High values occur

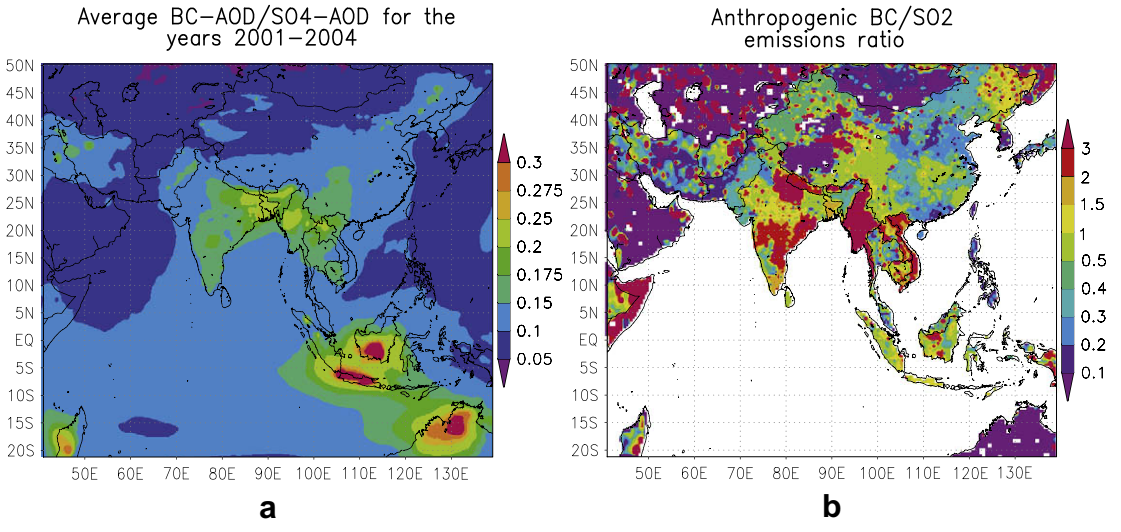

Fig. 8. (a) Ratio of BC to sulfate AOD distribution and (b) ratio of BC to SO_2 emissions.

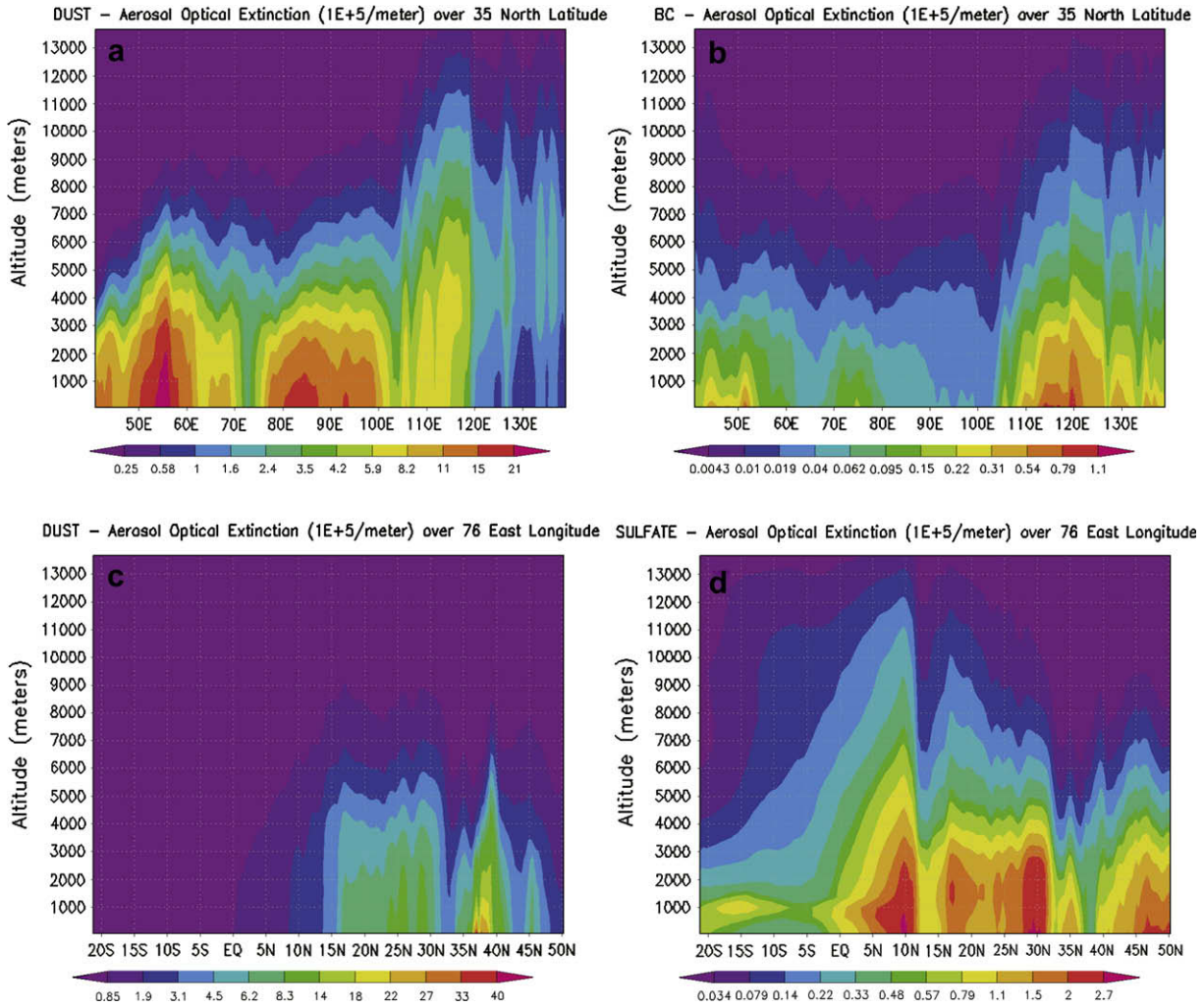

Fig. 9. Vertical structure of aerosols showing latitudinal and longitudinal gradients.

over the source areas (e.g., 30N). In the outflow region (south of 20N) the location of the maximum extinction occurs at altitudes 1–3 km, reflecting that the transport off the continent generally overrides the marine boundary layer.

3.3. Seasonal AOD distributions

The temporal variability of the aerosols at Hanimaadhoo, Maldives, and Gosan, Korea, for the 2001 and 2004 periods is shown in Figs. 10 and 11. These two sites are ideal to study the outflow of the Indian subcontinent and East Asia, respectively. Fig. 10a shows the time series of the vertical profiles of dust AOE along with the total column integrated dust AOD at Hanimaadhoo. The contribution from dust to AOD can reach up to ~0.2, and shows significant seasonal and inter-annual variability. The vertical profiles of dust AOE at Hanimaadhoo show significant seasonal changes in transport altitudes, with peak values in the July periods, with major contributions at altitudes ranging from 3 to 7 km. In contrast the anthropogenic aerosol loading at Hanimaadhoo, illustrated by the plots of sulfate AOE (BC and OC aerosols show similar trends) in Fig. 10b, shows that the sulfate loading is mainly at 3 km and lower altitudes, and with a different seasonality (peak in the dry season (JFM)). These differences in the dust and sulfate features reflect the different source regions and transport pathways for the wind blown dust and anthropogenic aerosols, as discussed in Adhikary et al. (2007).

Fig. 11 shows dust and BC AOE and AOD at Gosan. In general dust and BC have a similar seasonal cycle, with peak values in the spring, which is the strongest outflow period. At Gosan dust is transported at high altitudes, up to 9 km, while BC is typically confined mainly below the 4 km. Gobi and Taklimakan deserts in China, which are primary dust source regions impacting the atmosphere over Gosan, are further west from anthropogenic pollution sources located mostly in Eastern China. Furthermore the dust regions are at higher elevations than the bulk of the anthropogenic emissions which are nearer to the coast. Thus the results in Fig. 11 separating the vertical distribution of the dust layer from the pollution layer is as expected, with the dust outflow at higher altitudes than pollution aerosols such as

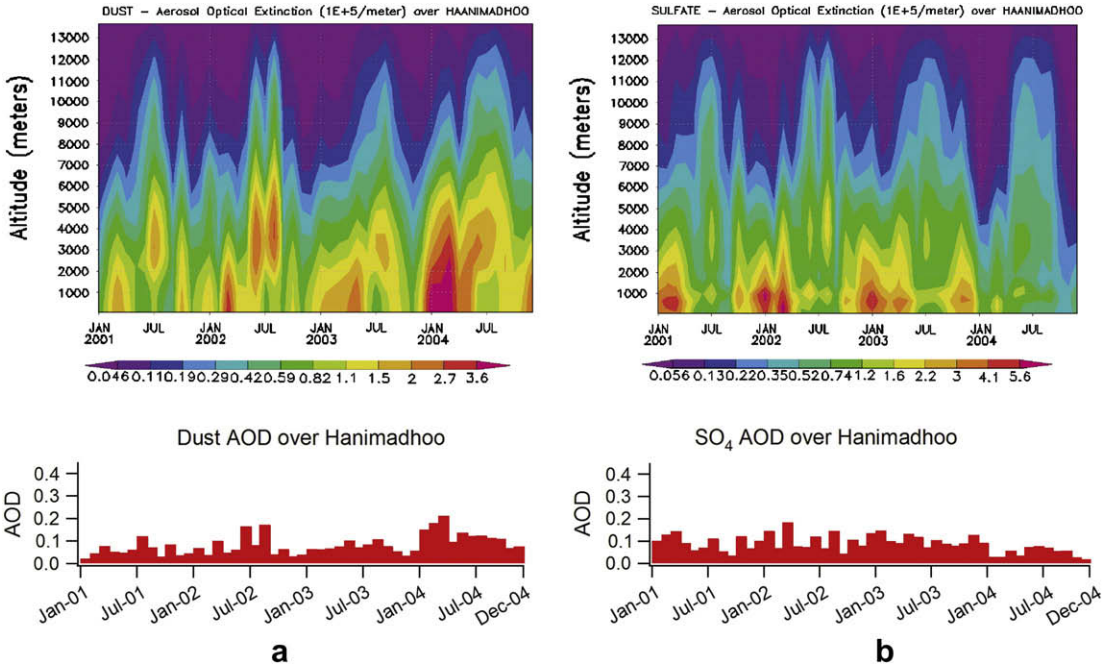

Fig. 10. Vertical structure and column integrated AOE at Hanimaadhoo.

BC. This separation of dust and pollution layers has also been observed using aircraft campaigns (Seinfeld et al., 2004; Stith et al., submitted for publication). However, since the assimilation algorithm does not constrain the vertical profile, the resulting vertical profiles are determined by the underlying chemical transport model.

3.4. Factor contribution: forward and receptor modeling

The results presented above in Figs. 11 and 12 indicate that the total AOD and the contributions from various species vary significantly by region and season. To help synthesize and characterize the contributions to AOD in

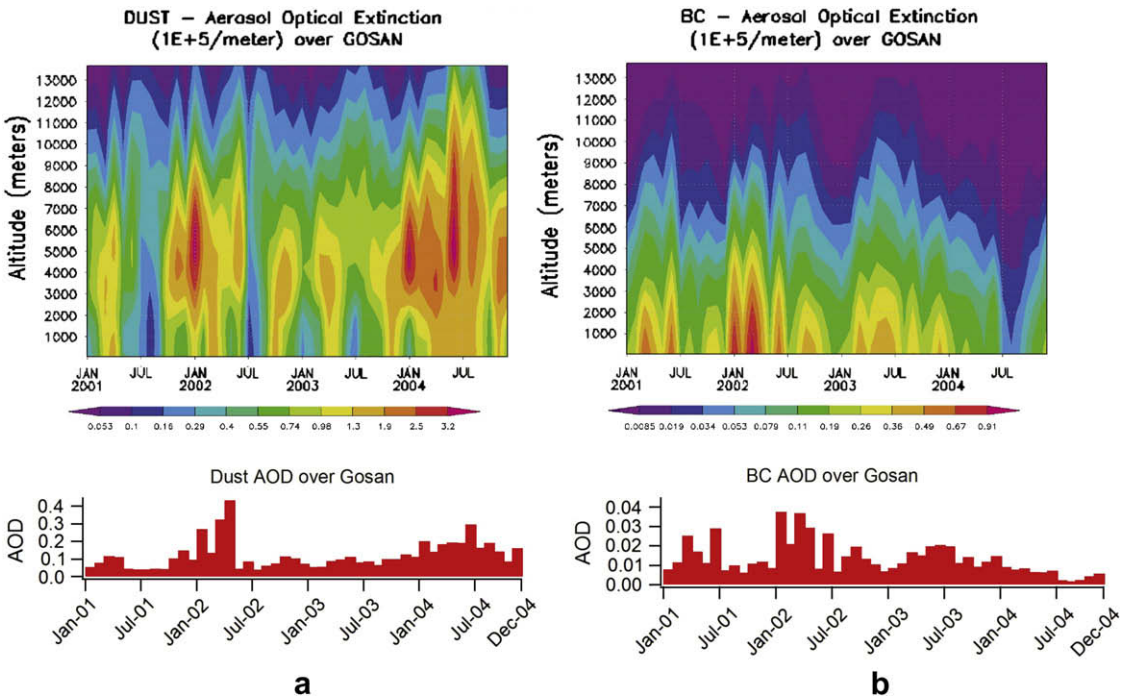

Fig. 11. Vertical structure and column integrated AOE at Gosan.

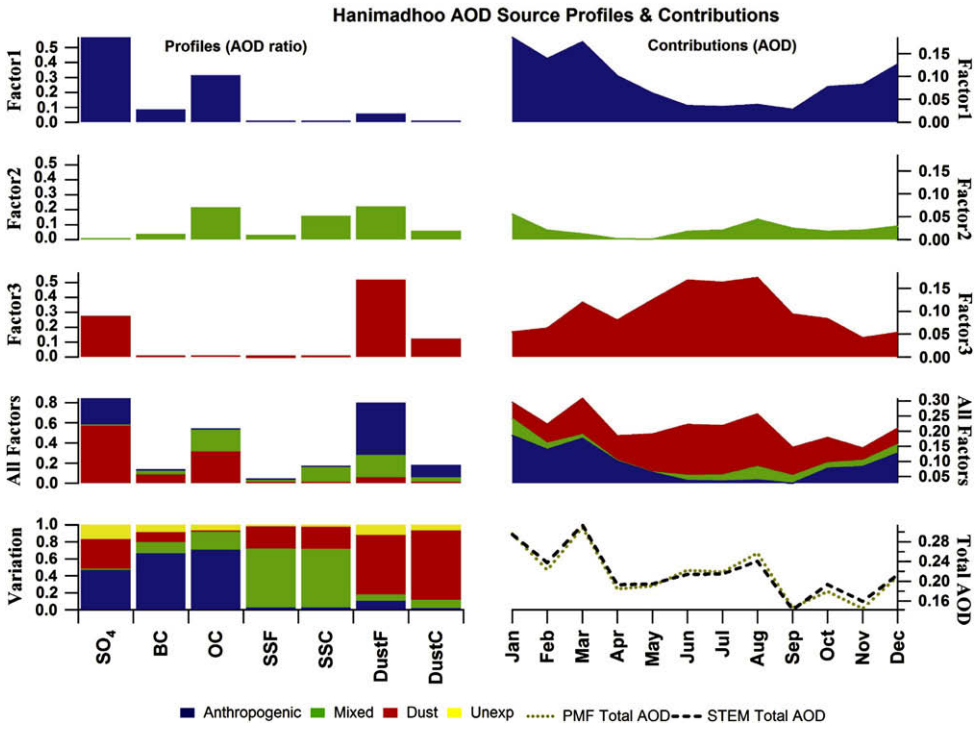

Fig. 12. PMF modeled aerosol profiles and contributions at Hanimaadhoo.

a particular region, we explored the application of PMF to the modeled constrained distributions to see if we could identify major source contributions. The application of PMF to model values provides a means to search for factors that can represent the source, transport and removal processes which link emissions, aerosol distributions and AOD. The four years of monthly mean AOD by species and size was treated in the PMF analysis. The general PMF guidelines including looking at *Q* and *EV* values and interpretability of the resolved sources were adhered to in obtaining the PMF solution. After careful examination of the various factor combinations, a three-factor solution was considered best to explain the variation in AOD while yielding physically meaningful factors. For example, a megacity located far from oceans and sand desert should not have a high factor loading of dust and sea salt as the factors that primarily explain the variation in AOD. We focus the discussion of PMF analysis on Gosan and Hanimaadhoo as these locations are influenced by the continental outflow from the Indian subcontinent and East Asia; thereby providing an opportunity to study the influence of diverse emission sources. We show here the averaged four-year contributions in order to better ascertain the influence of seasonality.

To illustrate, the resulting AOD factor profiles and contributions are displayed in Figs. 12 and 13. The output is arranged in a multi-panel plot format. The top three left and right panels in Figs. 12 and 13 correspond to the AOD profiles and contributions, respectively. The fourth panel in both figures shows the aggregate of profiles and contributions. The bottom left panel shows the variation explained in each species by the three factors. The bottom right panel shows a comparison of the PMF modeled AOD (which is sum of the individual factor contributions) with the total AOD from the assimilated STEM model.

The three-factor PMF solution for Hanimaadhoo is shown in Fig. 12. Factor 1 was identified as continental anthropogenic pollution factor (denoted by blue color) due to the strong association of SO_4, BC and OC in the profile (top left panel) and accounts for majority ($\sim$80%) of the variation in BC and OC along with a substantial portion of variation in SO_4 (bottom left panel). This factor peaks during the months of January and February (top right panel) consistent with the results of earlier studies (Ramanathan et al., 2007; Stone et al., 2007). Similarly we identified Factor 2 as mixed factor (denoted by green color) associated with OC, sea salt and dust (in second left panel) and explains most of the variation of sea salt species. This mixed factor shows a seasonal cycle with maximum contribution in July and August (second right panel). This period represents long-range transport from low latitudes, with long stretches over the sea, and generally from the areas influenced by outflow from Africa. This is in contrast to the seasonality of the first factor that reflects outflow from the Indian subcontinent. Like wise Factor 3 (denoted by red) was attributed to dust factor due to high dust loading (in third left panel) along with minor contributions of SO_4 and accounts for most of the variation in dust. This factor peaks occur through the months of May through August (third right panel), reflecting transport conditions bringing dust from the middle-east and the western regions of South Asia. A detailed discussion of the transport patterns impacting aerosol composition at Hanimaadhoo is

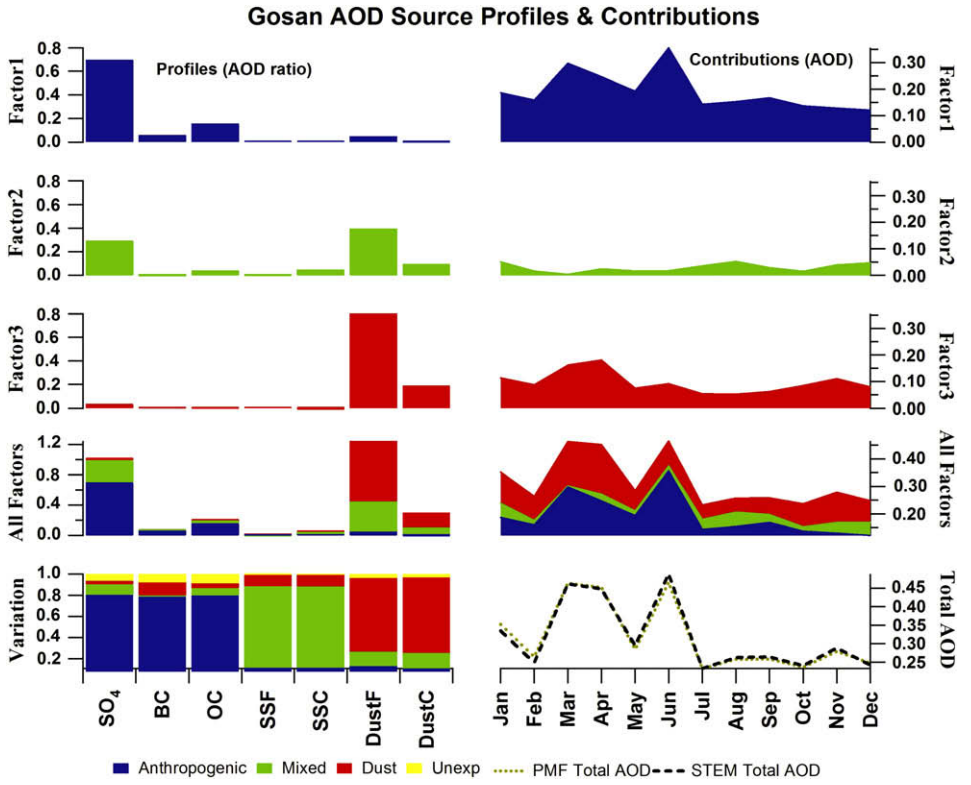

Fig. 13. PMF modeled aerosol profiles and contributions at Gosan.

presented by Adhikary et al. (2007). The PMF three-factor model explains more than 80% of the variation in the individual species as evident by the low values (<0.2) of unexplained variation of each species, denoted by yellow color (bottom left panel). This PMF solution explains 90% of the assimilated STEM total AOD as seen in the bottom right panel.

Fig. 13 shows the PMF results for Gosan. The following factors were identified: anthropogenic pollution source (denoted by blue color) dominated by sulfate, BC and OC, a mixed factor (denoted by green color), and a distinct dust factor (denoted by red color). The aerosol distributions at Gosan are dominated by pollution sources from East Asia, and 80% of the variation in sulfate, BC and OC is explained by the anthropogenic pollution sources (top left panel). The pollution factor also shows a significant contribution throughout the year, with maximum values in the winter and spring (top right panel). The variations within this period reflect changes in transport patterns, as well as removal processes (e.g., the decrease in AOD in May due to a springtime precipitation feature that occurs in this region at this time). The mixed pollution factor comprising sea salt, SO_4 and dust explains ~90% of the sea salt contribution to AOD, and its maximum contribution is in the summer months reflecting southerly transport conditions and aerosol distributions of lower latitude marine conditions. The sulfate contribution in this factor reflects the contribution from volcanic emissions to the south (including those from Kyushu, Japan). Most of the variation in the fine and coarse mode dust is explained by the dust factor (bottom left panel), which shows a distinct peak around the months of February through May (third right panel), reflecting the long-range transport of dust occurring due to springtime dust events. The total AOD calculated by PMF matches closely with the assimilated STEM total AOD as shown in the bottom right panel. This PMF solution could explain approximately 90% of the variation in each species as shown by the low values (<0.1) of the unexplained variation (yellow) in the bottom left panel.

Even though similar factors were identified at Gosan and Hanimaadhoo the composition of the factors varies significantly at the two locations. For instance, the dust factor at Hanimaadhoo includes traces of sulfate along with dust contributions. In contrast at Gosan, the dust factor is dominated by dust species. Differences can also be found in the composition of the anthropogenic pollution and mixed factors at the two locations. For example, the BC and OC contribution to the anthropogenic pollution factor profile is smaller at Gosan, while it has a more significant contribution at Hanimaadhoo. This is expected behavior since Hanimaadhoo is predominantly influenced by the continental outflow from the Indian subcontinent where the carbonaceous aerosol to SO_2 emissions are higher than in China as shown in Fig. 8b. Overall these differences in the factors reflect differences in regional emissions.

4. Summary

A framework for optimal interpolation of satellite data was used along with the STEM model to produce aerosol distributions in Asia for the four-year period 2001–2004

and April 2005. Aerosol optical depth and fine mode fraction information (where available) retrieved from the satellite-based MODIS instrument was used in the assimilation to produce AOD and aerosol mass distributions. The daily assimilation results were compared to AERONET data within the modeling domain and the assimilation scheme was shown to produce fields that more closely matched the observations. The assimilation of AOD was shown to improve the predictions of surface aerosol mass by comparison with independent PM mass measurements from South Asia. The assimilation of fine mode fraction of AOD was shown to significantly improve the prediction of $PM_{2.5}$ at the surface.

The temporal and spatial features of the four-year constrained aerosol distributions were analyzed. The regional distributions showed high aerosol loadings over regions with large anthropogenic emissions, including East Asia and the Ganges plains, areas with large open biomass burning (including South East Asia), and over the desert regions where wind blown soil emissions occur, including large regions in China and the middle-east. Dust emissions are highly uncertain and are not well constrained in the current data set due to a lack of AOD observations over the desert regions. The inter-annual CoV calculated from the data assimilated four-year AOD shows that most of the variance lies in areas dominated by wind blown dust and biomass burning. Analysis of the four-year averaged vertical structure of dust and anthropogenic aerosols show that dust is generally present at higher altitudes, while pollution at lower levels. The model is able to capture the observed trends of long-range aerosol transport when analyzing the longitudinal and latitudinal vertical cross sections.

Source receptor modeling was also conducted to help in identifying factors affecting two receptor sites Hanimaadhoo and Gosan in Asia. The three-factor PMF analysis at these two sites was able to capture the observed seasonal anthropogenic and dust loadings. The PMF results were also able to identify strong carbonaceous aerosol signal at Hanimaadhoo in contrast to Gosan representing the signature of different emissions outflow region.

The 2001–2004 year's three dimensional aerosol mass loadings from our data assimilated chemical transport model were used as inputs in calculating radiative forcing within the same modeling domain. The results of radiative forcing calculations and impacts over Asia are described in a paper by Chung et al. (submitted for publication).

The results from this study show that AOD assimilation can help reduce the uncertainty in the calculated aerosol distributions. The results also point out areas where the background model needs improvement. One important example is the improvement in the dust emissions algorithm, which overestimates dust emissions, especially in South Asia. The procedure will also benefit from improved AOD retrievals. For example, MODIS products over the desert and other bright reflecting surface areas such as the 'Deep Blue' based retrieval should greatly assist in reducing the uncertainty over the desert regions. In addition, the retrieval of additional information other than size that can be used to distinguish between aerosol components (such as SSA) will also improve the assimilation and resulting aerosol distributions. This information should also be used to weight the assimilation factor between the different fine mode AOD fractions instead of linear adjustment as was done in our study. In future, PMF results at various different receptor locations showing factor profiles and contributions to the total observed AOD should help constrain the assimilation model further in differentiating between various fine mode aerosols.

Acknowledgements

We would like to thank the various PIs of AERONET sites in maintaining their sites so that we can use their AOD and angstrom exponent data. This work was supported by a NASA grant (NNG04GC58 G). The Pacific Northwest National Laboratory is operated for the U.S. Department of Energy by Battelle Memorial Institute under Contract DE-AC06-76RLO 1830.

References

Adhikary, B., Carmichael, G.R., Tang, Y., Leung, L.R., Qian, Y., Schauer, J.J., Stone, E.A., Ramanathan, V., Ramana, M.V., 2007. Characterization of the seasonal cycle of south Asian aerosols: a regional-scale modeling analysis. Journal of Geophysical Research 112.

Anderson, T.L., Charlson, R.J., Bellouin, N., Boucher, O., Chin, M., Christopher, S.A., Haywood, J., Kaufman, Y.J., Kinne, S., Ogren, J.A., Remer, L.A., Takemura, T., Tanre, D., Torres, O., Trepte, C.R., Wielicki, B. A., Winker, D.M., Yu, H., 2005. An "A-Train" strategy for quantifying direct climate forcing by anthropogenic aerosols. Bulletin of the American Meteorological Society 86 (12), 1795–1809.

Bates, T.S., Anderson, T.L., Baynard, T., Bond, T., Boucher, O., Carmichael, G., Clarke, A., Erlick, C., Guo, H., Horowitz, L., Howell, S., Kulkarni, S., Maring, H., McComiskey, A., Middlebrook, A., Noone, K., O'Dowd, C.D., Ogren, J., Penner, J., Quinn, P.K., Ravishankara, A.R., Savoie, D.L., Schwartz, S.E., Shinozuka, Y., Tang, Y., Weber, R.J., Wu, Y., 2006. Aerosol direct radiative effects over the northwest Atlantic, northwest Pacific, and north Indian Oceans: estimates based on in-situ chemical and optical measurements and chemical transport modeling. Atmospheric Chemistry and Physics 6 (6), 1657–1732.

Bond, T.C., Streets, D.G., Yarber, K.F., Nelson, S.M., Woo, J.-H., Klimont, Z., 2004. A technology-based global inventory of black and organic carbon emissions from combustion. Journal of Geophysical Research – Atmospheres 109 (D14) D14203/1–D14203/43.

Carmichael, G.R., Tang, Y., Kurata, G., Uno, I., Streets, D., Woo, J.H., Huang, H., Yienger, J., Lefer, B., Shetter, R., Blake, D., Atlas, E., Fried, A., Apel, E., Eisele, F., Cantrell, C., Avery, M., Barrick, J., Sachse, G., Brune, W., Sandholm, S., Kondo, Y., Singh, H., Talbot, R., Bandy, A., Thorton, D., Clarke, A., Heikes, B., 2003. Regional-scale chemical transport modeling in support of the analysis of observations obtained during the TRACE-P experiment. Journal of Geophysical Research – Atmospheres 108 (D21) GTE44/1–GTE44/28.

Chai, T., Carmichael, G.R., Tang, Y., Sandu, A., Hardesty, M., Pilewskie, P., Whitlow, S., Browell, E.V., Avery, M.A., Nédélec, P., 2007. Four-dimensional data assimilation experiments with International Consortium for Atmospheric Research on Transport and Transformation ozone measurements. Journal of Geophysical Research 112.

Chameides, W.L., Yu, H., Liu, S.C., Bergin, M., Zhou, X., Mearns, L., Wang, G., Kiang, C.S., Saylor, R.D., Luo, C., Huang, Y., Steiner, A., Giorgi, F., 1999. Case study of the effects of atmospheric aerosols and regional haze on agriculture: an opportunity to enhance crop yields in China through emission controls? Proceedings of the National Academy of Sciences of the United States of America 96 (24), 13626–13633.

Chueinta, W., Hopke, P.K., Paatero, P., 2000. Investigation of sources of atmospheric aerosol at urban and suburban residential areas in Thailand by positive matrix factorization. Atmospheric Environment 34 (20), 3319–3329.

Chung, C.E., Ramanathan, V., Kim, D., Podgorny, I.A., 2005. Global anthropogenic aerosol direct forcing derived from satellite and ground-based observations. Journal of Geophysical Research 110.

Chung, C.E., Ramanathan, V., Carmichael G.R., Tang, Y., Adhikary, B., Leung, L.R., Qian, Y. Anthropogenic aerosol radiative forcing in Asia derived from regional models with atmospheric and aerosol data

assimilation. Journal of Geophysical Research, submitted for publication.
Collins, W.D., Rasch, P.J., Eaton, B.E., Khattatov, B.V., Lamarque, J.-F., Zender, C.S., 2001. Simulating aerosols using a chemical transport model with assimilation of satellite aerosol retrievals: methodology for INDOEX. Journal of Geophysical Research – Atmospheres 106 (D7), 7313–7336.
Gautam, R., Hsu, N.C., Kafatos, M., Tsay, S.C., 2007. Influences of winter haze on fog/low cloud over the Indo-Gangetic plains. Journal of Geophysical Research 112, D05207.
Gong, S.L., 2003. A parameterization of sea-salt aerosol source function for sub- and super-micron particles. Global Biogeochemical Cycles 17 (4) 8/1–8/7.
Guttikunda, S.K., Tang, Y., Carmichael, G.R., Kurata, G., Pan, L., Streets, D.G., Woo, J.-H., Thongboonchoo, N., Fried, A., 2005. Impacts of Asian megacity emissions on regional air quality during spring 2001. Journal of Geophysical Research – Atmospheres 110 (D20) D20301/1–D20301/18, 8 plates.
Hsu, N.C., Tsay, S.C., King, M.D., Herman, J.R., 2006. Deep Blue retrievals of Asian aerosol properties during ACE-Asia. IEEE Transactions on Geoscience and Remote Sensing 44 (11), 3180.
Huebert, B.J., Bates, T., Russell, P.B., Shi, G., Kim, Y.J., Kawamura, K., Carmichael, G., Nakajima, T., 2003. An overview of ACE-Asia: strategies for quantifying the relationships between Asian aerosols and their climatic impacts. Journal of Geophysical Research – Atmospheres 108 (D23) ACE1/1–ACE1/20.
IGAC, 2007. Special Issue on Satellite Retrievals of Tropospheric Chemistry. Newsletter of the International Global Atmospheric Chemistry Project March 2007 (Issue No. 35).
IPCC, 2007. Contribution of Working Group I to the Fourth Assessment Report of the Intergovernmental Panel on Climate Change. In: Solomon, S., Qin, D., Manning, M. (Eds.), Climate Change 2007: the Physical Science Basis. Cambridge University Press, Cambridge, United Kingdom and New York, NY, USA.
Jacobson, M.Z., 2005. Fundamentals of Atmospheric Modeling. Cambridge University Press, Cambridge, UK; New York.
Jeuken, A.B.M., Eskes, H.J., Van Velthoven, P.F.J., Kelder, H.M., Holm, E.V., 1999. Assimilation of total ozone satellite measurements in a three-dimensional tracer transport model. Journal of Geophysical Research – Atmospheres 104 (D5), 5551–5563.
Juntto, S., Paatero, P., 1994. Analysis of daily precipitation data by Positive Matrix Factorization. Environmetrics 5 (2), 127–144.
Kalnay, E., 2003. Atmospheric Modeling, Data Assimilation and Predictability. Cambridge University Press, Cambridge.
Khattatov, B.V., Lamarque, J.-F., Lyjak, L.V., Menard, R., Levelt, P., Tie, X., Brasseur, G.P., Gille, J.C., 2000. Assimilation of satellite observations of long-lived chemical species in global chemistry transport models. Journal of Geophysical Research – Atmospheres 105 (D23), 29135–29144.
Kim, E., Hopke, P.K., Kenski, D.M., Koerber, M., 2005. Sources of fine particles in a rural Midwestern US area. Environmental Science & Technology 39 (13), 4953–4960.
Kinne, S., Schulz, M., Textor, C., Guibert, S., Balkanski, Y., Bauer, S.E., Berntsen, T., Berglen, T.F., Boucher, O., Chin, M., 2006. An AeroCom initial assessment – optical properties in aerosol component modules of global models. Atmospheric Chemistry and Physics 6, 1815–1834.
Lamarque, J.F., Khattatov, B.V., Gille, J.C., 2002. Constraining tropospheric ozone column through data assimilation. Journal of Geophysical Research – Atmospheres 107 (D22) ACH9/1–ACH9/11.
Lee, E., Chan, C.K., Paatero, P., 1999. Application of positive matrix factorization in source apportionment of particulate pollutants in Hong Kong. Atmospheric Environment 33 (19), 3201–3212.
Lorenc, A.C., 1986. Analysis methods for numerical weather prediction. Quarterly Journal of the Royal Meteorological Society 112 (474), 1177–1194.
Niu, T., Gong, S.L., Zhu, G.F., Liu, H.L., Hu, X.Q., Zhou, C.H., Wang, Y.Q., Zhang, X.Y., 2007. Data assimilation of dust aerosol observations for CUACE/dust forecasting system. Atmospheric Chemistry and Physics Discussion 7, 8309–8332.
Olivier, J.G.J., Berdowski, J.J.M., 2001. In: Berdowski, J., Guicherit, R., Heij, B. J. (Eds.), Global Emissions Sources and Sinks. The Climate System. A.A. Balkema Publishers/Swets & Zeitlinger Publishers, The Netherlands, pp. 33–78.
Paatero, P., 2000. User's Guide for Positive Matrix Factorization Programs PMF2 and PMF3.
Paterson, K.G., Sagady, J.L., Hooper, D.L., 1999. Analysis of air quality data using positive matrix factorization. Environmental Science & Technology 33 (4), 635–641.
Penner, J.E., Andrae, M., Annegarn, H., Barrie, L., Feichter, J., Hegg, D., Jayaraman, A., Leaitch, R., Murphy, D., Nganga, J., Pitari, G., 2001. Aerosols, their Direct and Indirect Effects (Chapter 5) in Climate Change 2001: the Scientific Basis: Contribution of Working Group I to the Third Assessment Report of the Intergovernmental Panel on Climate Change, Cambridge University Press.
Polissar, A.V., Hopke, P.K., Paatero, P., Kaufmann, Y.J., Hall, D.K., Bodhaine, B.A., Dutton, E.G., Harris, J.M., 1999. The aerosol at Barrow, Alaska: long-term trends and source locations. Atmospheric Environment 33 (16), 2441–2458.
Pope III, C.A., Burnett, R.T., Thun, M.J., Calle, E.E., Krewski, D., Ito, K., Thurston, G.D., 2002. Lung cancer, cardiopulmonary mortality, and long-term exposure to fine particulate air pollution. The Journal of the American Medical Association 287 (9), 1132–1141.
Ramanathan, V., Carmichael, G., 2008. Global and regional climate changes due to black carbon. Nature Geoscience 1 (4), 221.
Ramanathan, V., Crutzen, P.J., Kiehl, J.T., Rosenfeld, D., 2001a. Atmosphere aerosols, climate, and the hydrological cycle (Washington, DC, United States). Science 294 (5549), 2119–2124.
Ramanathan, V., Crutzen, P.J., Lelieveld, J., Mitra, A.P., Althausen, D., Anderson, J., Andreae, M.O., Cantrell, W., Cass, G.R., Chung, C.E., Clarke, A.D., Coakley, J.A., Collins, W.D., Conant, W.C., Dulac, F., Heintzenberg, J., Heymsfield, A.J., Holben, B., Howell, S., Hudson, J., Jayaraman, A., Kiehl, J.T., Krishnamurti, T.N., Lubin, D., McFarquhar, G., Novakov, T., Ogren, J.A., Podgorny, I.A., Prather, K., Priestley, K., Prospero, J.M., Quinn, P.K., Rajeev, K., Rasch, P., Rupert, S., Sadourny, R., Satheesh, S.K., Shaw, G.E., Sheridan, P., Valero, F.P.J., 2001b. Indian ocean experiment: an integrated analysis of the climate forcing and effects of the great Indo-Asian haze. Journal of Geophysical Research – Atmospheres 106 (D22), 28371–28398.
Ramanathan, V., Li, F., Ramana, M.V., Praveen, P.S., Kim, D., Corrigan, C.E., Nguyen, H., Stone, E.A., Schauer, J.J., Carmichael, G.R., Adhikary, B., Yoon, S.C., 2007. Atmospheric brown clouds: hemispherical and regional variations in long-range transport, absorption, and radiative forcing. Journal of Geophysical Research 112 (D22).
Seinfeld, J.H., Carmichael, G.R., Arimoto, R., Conant, W.C., Brechtel, F.J., Bates, T.S., Cahill, T.A., Clarke, A.D., Doherty, S.J., Flatau, P.J., 2004. ACE-ASIA: regional climatic and atmospheric chemical effects of Asian dust and pollution. Bulletin of the American Meteorological Society 85 (3), 367–380.
Stith, J.L., Cooper, W.A., Roberts, G., DeMott, P., Carmichael, G., Hatch, C., Adhikary, B., Twohy, C., Rogers, D.C., Campos, T., Baumgardner, D., Gao, R. Cross-pacific transport of Asian dust-mode particles and cloud active nuclei. Journal of Geophysical Research, submitted for publication.
Stone, E.A., Lough, G.C., Schauer, J.J., Praveen, P.S., Corrigan, C.E., Ramanathan, V., 2007. Understanding the origin of black carbon in the atmospheric brown cloud over the Indian Ocean. Journal of Geophysical Research 112 (D22).
Streets, D.G., Bond, T.C., Carmichael, G.R., Fernandes, S.D., Fu, Q., He, D., Klimont, Z., Nelson, S.M., Tsai, N.Y., Wang, M.Q., Woo, J.H., Yarber, K.F., 2003. An inventory of gaseous and primary aerosol emissions in Asia in the year 2000. Journal of Geophysical Research – Atmospheres 108 (D21) GTE30/1–GTE30/23.
Tang, Y., Carmichael, G.R., Kurata, G., Uno, I., Weber, R.J., Song, C.-H., Guttikunda, S.K., Woo, J.-H., Streets, D.G., Wei, C., Clarke, A.D., Huebert, B., Anderson, T.L., 2004. Impacts of dust on regional tropospheric chemistry during the ACE-Asia experiment: a model study with observations. Journal of Geophysical Research – Atmospheres 109 (D19) D19S21/1–D19S21/21.
Uno, I., Carmichael, G.R., Streets, D.G., Tang, Y., Yienger, J.J., Satake, S., Wang, Z., Woo, J.-H., Guttikunda, S., Uematsu, M., Matsumoto, K., Tanimoto, H., Yoshioka, K., Iida, T., 2003. Regional chemical weather forecasting system CFORS: model descriptions and analysis of surface observations at Japanese island stations during the ACE-Asia experiment. Journal of Geophysical Research – Atmospheres 108 (D23) ACE36/1–ACE36/17.
Wang, J., Nair, U.S., Christopher, S.A., 2004. GOES 8 aerosol optical thickness assimilation in a mesoscale model: online integration of aerosol radiative effects. Journal of Geophysical Research 109, D23203.
van der Werf, G.R., Randerson, J.T., Giglio, L., Collatz, G.J., Kashibhatla, P.S., 2006. Interannual variablility in global biomass burning emissions from 1997 to 2004. Available from: http://ess1.ess.uci.edu/%7Ejranders/data/GFED2/ (accessed 3.16.2006.).
Yu, H., Dickinson, R.E., Chin, M., Kaufman, Y.J., Geogdzhayev, B., Mishchenko, M.I., 2003. Annual cycle of global distributions of aerosol optical depth from integration of MODIS retrievals and GOCART model simulations. Journal of Geophysical Research 108, 4128.